Catalysis Science & Technology

Accepted Manuscript

This article can be cited before page numbers have been issued, to do this please use: W. Tang, L. Chen, J. Deng, Y. Kuang, C. Chen, B. Yin, H. Wang, J. Lin and D. Wei, *Catal. Sci. Technol.*, 2020, DOI: 10.1039/D0CY01411G.




ROYAL SOCIETY OF CHEMISTRY

rsc.li/catalysis

View Article Online
DOI: 10.1039/D0CY01411G

ARTICLE

# Structure-guided evolution of carbonyl reductase for efficient biosynthesis of ethyl (*R*)-2-hydroxy-4-phenylbutyrate

Received 00th January 20xx,
Accepted 00th January 20xx

DOI: 10.1039/x0xx00000x

Wen Tang[a], Lulu Chen[a], Jian Deng[a], Yuyao Kuang[a], Chao Chen[b], Bo Yin[c], Hualei Wang[a], Jinping Lin*[a], Dongzhi Wei[a]

Ethyl (*R*)-2-hydroxy-4-phenylbutanoate ((*R*)-HPBE) is an important versatile intermediate for the synthesis of angiotensin-converting enzyme inhibitors. Herein, a structure-guided rational design was adopted to improve the catalytic performance of carbonyl reductase from *Gluconobacter oxydans* (*Go*CR) for efficient production of (*R*)-HPBE at high substrate loading. To enhance the catalytic performance of *Go*CR, three sites (Cys93, Ile187 and Trp193) were identified based on computational approach. Through single-site and cooperative mutation at these three sites, four variants with simultaneous increase in stereoselectivity and catalytic efficiency were obtained. Variant mut-W193L, mut-W193L/C93I, mut-W193L/I187L and mut-W193L/C93I/I187L exhibited 9.8- to 37.0-fold increase in catalytic efficiency ($k_{cat}/K_m$) compared to wild-type enzyme. Meanwhile, stereoselectivities of these variants were improved from 43.0% *ee* of wild-type *Go*CR to >99% *ee*. Besides, mut-W193L/C93I/I187L displayed the improved thermostability simultaneously. Theoretical structural analysis revealed that the changes of catalytic pocket microenvironment resulted in the concurrent improvement of enzyme activity and thermostability. In the batch production of (*R*)-HPBE, up to 371 g/L substrate loading was completely reduced utilizing the most efficient variant mut-W193L/C93I/I187L at 40°C, affording (*R*)-HPBE with >99% *ee* and a space-time yield of 540.4 g/(L·day). This study provides a potential and attractive biocatalyst for the efficient synthesis of (*R*)-HPBE.

## Introduction

Chiral alcohols are important and useful building blocks for the synthesis of various agrochemicals, aroma chemicals, flavours, food, pharmaceuticals and specialty materials [1-3]. Among them, ethyl (*R*)-2-hydroxy-4-phenylbutanoate ((*R*)-HPBE) is a versatile key precursor for the synthesis of angiotensin-converting enzyme (ACE) inhibitors, known as commercial "prils" [4]. To date, a series of methods have been developed for the preparation of (*R*)-HPBE, including chemical and enzymatic asymmetric reduction of ethyl 2-oxo-4-phenyl-butyrate (OPBE) [5,6], kinetic resolution of the corresponding racemate [7,8], enzymatic esterification of 2-hydroxy-4-phenylbutanoic acid [9] and chemical multi-step synthesis [10]. In contrast, carbonyl reductase-mediated asymmetric reduction of OPBE to (*R*)-HPBE has been an attractive method due to its significant advantages such as high yield, high economic feasibility, environmental benignity and under mild reaction conditions [4,11].

An increasing number of carbonyl reductases and dehydrogenases have been discovered in recent years to synthesize (*R*)-HPBE, but most naturally occurring enzymes showed low catalytic activity, limited stereoselectivity, poor stability, or poor tolerance for high substrate concentrations, restricting their practical application [12-16]. So far, only a few examples of robust carbonyl reductases have been reported that could catalyse OPBE at high substrate concentration. One of the successful examples is a carbonyl reductase CgKR2 from *Candida glabrata* which was found to completely reduce 206 g/L OPBE to (*R*)-HPBE with 99% *ee* [17]. In addition, the recombinant *E. coli* cells overexpressing a carbonyl reductase IolS from *B. subtilis* and glucose dehydrogenase (GDH) were employed in preparing (*R*)-HPBE with 99% *ee* and 100% conversion at 330 g/L OPBE [11]. However, these cases at present still cannot meet the needs of practical production. These indicate that developing and redesigning robust biocatalysts and subsequently performing biocatalytic reduction process at high substrate concentrations have always been an ongoing subject.

Protein engineering such as de novo enzyme design, structure-guided (semi-) rational design and directed evolution, has been employed to address these undesirable properties of enzymes mentioned above and to remould the enzymatic property of enzymes [18-21]. With the rapid development of bioinformatics data bases including computational chemistry and gene sequence/three-dimensional structures of proteins, the structure-guided (semi-)rational design strategy has been the

[a] State Key Laboratory of Bioreactor Engineering, New World Institute of Biotechnology, East China University of Science and Technology, No.130 Meilong Road, Shanghai 200237, People's Republic of China. E-mail: jplin@ecust.edu.cn
[b] State Key Laboratory of Bioreactor Engineering, Biomedical Nanotechnology Center, School of Biotechnology, East China University of Science and Technology, Shanghai 200237, People's Republic of China.
[c] National University of Singapore (Suzhou) Research Institute, No. 377 Linquan Street, Suzhou Industrial Park, Suzhou215123, Jiangsu, People's Republic of China.
Electronic Supplementary Information (ESI) available: [details of any supplementary information available should be included here]. See DOI: 10.1039/x0xx00000x

preferred choice because of smaller mutant libraries and reduced labor as well as process time. Regarding (semi-)rational design, various enzymes, including carbonyl reductases, have been successfully tailored to improve catalytic activity [22,23] or thermostability [24,25], to improve or invert stereoselectivity [6,23,26] and to broaden the scope of substrates accepted [23,27]. As a result, more efficient enzymes for chiral alcohol synthesis have been designed and produced through structure-guided rational design.

Previously, we identified a NAD(H)-dependent short-chain dehydrogenase from *Gluconobacter oxydans* (*Go*CR), which displayed a broad substrate spectrum, and in particular, exhibited the great potential in reduction of halogenated acetophenones to the corresponding (*S*)-alcohols with exclusive Prelog-selectivity (>99% *ee*) [26,28]. To probe the molecular mechanism of stereoselectivity, we solved the crystal structure of *Go*CR (PDB ID: 3WTC), and found Trp193 site played the critical role in determining stereoselectivity. Consequently, a single-site mutant W193A was constructed by rational design, and this mutant enzyme was proved to reduce OPBE to (*R*)-HPBE with a significantly improved *ee* of >99% compared to 43.2% for the wild type [26]. Despite this success, the low activity of the variant mut-W193A limited its application. Herein, we attempted to engineer *Go*CR via structure-guided semi-rational design for improved catalytic performance in asymmetric reduction of OPBE at high substrate loading. Computer-aided structural analysis was also employed to understand the potential mechanism for the improved performance of variants. Finally, the production of (*R*)-HPBE employing *E. coli* cells co-expressing *Go*CR variants and glucose dehydrogenase was also evaluated.

## Experimental

### Materials

Strains Genomic DNA of *Gluconobacter oxydans* strain 621H was used as the template for PCR amplification of *Go*CR gene. Escherichia coli (*E. coli*) BL21 (DE3) cells and pET-28a (+) vector (Novagen, Shanghai, China) were used for over-expression of wild-type *Go*CR, its variants and glucose dehydrogenase. Oligonucleotide primers used for mutagenesis were synthesized at Sangni Biotech. (Shanghai, China). HPLC reagents hexane, 2-propanol and chemicals ethyl 2-oxo-4-phenyl-butyrate (OPBE) as well as ethyl (*R*)-2-hydroxy-4-phenylbutanoate ((*R*)-HPBE) were obtained from Adamas Reagent Co., Ltd. (Shanghai, China). Ethyl (*S*)-2-hydroxy-4-phenylbutanoate ((*S*)-HPBE) was purchased from Yuanye Bio-Technology Co. Ltd (Shanghai, China). Reduced β-nicotinamide adenine diphosphate (NADH) and β-nicotinamide adenine diphosphate ($NAD^+$) were purchased from Jierui Reagent Co., Ltd. (Shanghai, China). Other chemicals involved were analytical grade and commercially available.

### Site-directed mutagenesis

Site-directed mutagenesis was conducted using the mutation primers (presented in Table S1) according to the manufacturer's instructions of KOD-Plus-Mutagenesis Kit (Toyobo, Japan), and the pET-28a (+) vector harbouring *Go*CR gene was used as template. Subsequently, the recombinant plasmids harbouring *Go*CR or its mutant gene were transformed into *E. coli* DH5α competent cells. Afterwards, the colonies after transformation were selected for DNA sequencing to obtain all designed variants. After that, the recombinant plasmids harbouring designed variants were extracted from *E. coli* DH5α cells and then transformed into *E. coli* BL21 (DE3) competent cells for enzyme expression.

### Protein expression and purification

The *E. coli* BL21 (DE3) cells harbouring recombinant plasmids of *Go*CR or its variants were cultured in 5 mL of LB medium containing 50 μg/mL kanamycin at 37°C. Subsequently, such overnight culture was inoculated into 200 mL LB medium and cultured at 37°C. When the optical density ($OD_{600}$) of culture reached to around 0.6, isopropyl-β-D-thiogalactopyranoside (IPTG) with 0.25 mM final concentration was added to induce enzyme expression at 30°C for another 10 h. After induction completion, the recombinant *E. coli* cells were centrifuged at 4°C (6000 ×g, 15 min), washed with 0.9% NaCl solution for several times and stored at -40°C.

The collected recombinant *E. coli* cells were resuspended in PBS (100 mM, pH 7.4 ), and then disrupted through ultrasonication in an ice water bath, followed by centrifugation (12000 ×g, 30 min, 4°C) to collect supernatant. Subsequently, supernatant was filtered by 0.45 μm hydrophilic membranes, and then loaded onto a 5 mL HisTrap FF crude column pre-equilibrated with 20 mM imidazole in PBS (100 mM, pH 7.4). The fractions were collected by gradient elution with an increasing concentration (20-500 mM) of imidazole in PBS (100 mM, pH 7.4). Fractions containing the target protein were verified by SDS-PAGE analysis and collected. The collections were dialyzed with PBS (20 mM, pH 7.4) containing 200 mM NaCl and 5% (v/v) glycerinum for desalting, and then concentrated by Millipore (3 KDa). The purity of target protein was checked by SDS-PAGE. The enzyme concentration was determined by the standard Bradford's method [29].

### Enzyme activity assay, kinetic parameter and catalytic efficiency determination

The enzyme activities of *Go*CR and its variants were determined by monitoring the change in NADH absorbance at 340 nm using a microplate reader (SpectraMax190, Molecular Devices, USA). The standard assay mixture (0.2 mL) consisted of PBS (100 mM, pH 7.4), 0.2 mM NADH, 10 mM substrate and appropriate diluted enzyme. All reactions except as specified were pre-mixed at 30°C and initiated by adding NADH. One unit of enzyme activity was defined as the amount of enzyme that catalyzes the oxidation of 1.0 μmol NADH per minute.

The kinetic parameters of purified *Go*CR and its variants towards substrate OPBE were determined by measuring the activity at different substrate concentrations (0.1-2.0 mM) with a fixed NADH concentration of 0.2 mM. Initial velocity data obtained were fitted to the Michaelis-Menten equation. The Michaelis constant $K_m$ and the maximum velocity $V_{max}$ were calculated by using Lineweaver-Burk plots.

For comparison of stereoselectivity and catalytic activity of *Go*CR variants, OPBE (0.5 M), D-glucose (0.6 M), lyophilized *E. coli* cells harbouring *Go*CR variants (20 g/L), lyophilized *E. coli* cells harbouring $GDH_{E170K/Q252L}$ (20 g/L), octanol (10%), $NAD^+$ (0.5 mM) and phosphate buffer (100 mM, pH 7.5) were combined. The reaction was carried out at 30°C and 200 rpm for 1 h. The conversion and stereoselectivity were determined by Gas Chromatography (GC) and High Performance Liquid Chromatography (HPLC), respectively. For easy comparison purpose, conversion of the control (mut-W193L) was set as 100%.

**Circular dichroism spectroscopy studies**

Secondary structural analysis by circular dichroism (CD) spectra at different temperatures can be used to provide information about enzyme stability [30]. The CD spectra of *Go*CR and its variants were measured by a Chirascan CD spectrometer (Applied Photophysics Ltd., Leatherhead, UK) equipped with a TC125 temperature-control system (Quantum Northwest, Liberty Lake, WA, USA). The unfolding curves were measured from 200 to 260 nm against gradient temperatures, using the temperature scan mode with a gradient of 1°C/min. The purified enzyme was diluted to 1.0-1.5 mg/mL in 20 mM sodium phosphate buffer (pH 7.4). The melting temperature ($T_m$) values were calculated by Global 3 analysis software (Applied Photophysics, UK).

**Computational analysis**

According to previous studies [31-34], we chose the conformation of enzyme-substrate complex after energy minimization to calculate the binding free energy. Here, considering the reason that reaction enthalpy that is presumably driven by hydrogen bonding interaction between enzyme and substrate is the major thermodynamic factor, we used relative binding free energy (without entropy) to assess the relative importance of different amino acid residues in substrate binding, which had also been used in the previous study [35]. Specifically, the relative binding free energy ($\triangle G_{bind}$ in kcal/mol) of mut-W193L-OPBE complex after energy minimization was estimated by the Molecular Mechanics Generalized Born Surface Area (MM-GBSA) module implemented in AmberTools 14. Subsequently, the per-residue binding free energy decomposition was performed to identify the potential residues responsible for substrate binding process.

The virtual variants (mut-W193L, mut-W193L/C93I, mut-W193L/I198L and mut-W193L/C93I/I187L) of *Go*CR (PDB ID: 3WTC) were firstly constructed by free PyMoL-edu. Then, molecular docking between *Go*CR or its variants and OPBE was conducted by the AutoDock1.5.6 program. The detailed parameters were set according to our previous study except the following modification [26]. In particular, the substrate OPBE, Cys93, Ile187 and catalytic tetrad (Asn113-Ser142-Tyr155-Lys159) were set as flexible, while the other residues in variants were set as rigid. The enzyme-substrate conformation with the lowest binding energy was further analyzed by PyMoL-edu. Besides, the interactions of residues at positions 93, 187 and 193 site with other residues in *Go*CR or its variants were studied through the RING 2.0 web server (http://protein.bio.unipd.it/ring/) [36].

**Co-expressing of *Go*CR variant and glucose dehydrogenase in *E. coli* cells**

A one-plasmid co-expression system of *Go*CR variant and $GDH_{E170K/Q252L}$ was constructed using the primers listed in Table S2. Briefly, a thermostable glucose dehydrogenase gene ($GDH_{E170K/Q252L}$) [37,38] as constructed in vector pET-28a (+) (pET28a-*GDH*) using the primers listed in Table S2, entry 1, 2. Meanwhile, the gene (*mutant*) of *Go*CR mutant was cloned in vector pET-28a (+) (pET28a-*mutant*) using the primers listed in Table S2, entry 3, 4. Subsequently, the $GDH_{E170K/Q252L}$ gene was amplified by PCR using primers with pET28a-$GDH_{E170K/Q252L}$ as a template and cloned into Hind III/Xhol I sites of vector pET28a-*mutant* (Table S2, entry 5, 6). As a result, genes *mutant* and $GDH_{E170K/Q252L}$ were arranged in tandem in one-plasmid pET28a (+), which was under the control of a separate T7 promoter and terminator, respectively.

**Asymmetric reduction of OPBE**

The whole-cell bioreduction of OPBE was conducted in a two-liquid (octanol : PBS = 15:85, v/v) 10-mL biphase reaction system which contained octanol (15%), PBS (100 mM, pH 7.5), OPBE (1.5-1.8 M), D-glucose (1.2 equiv.), lyophilized *E. coli* cells co-expressing *Go*CR variant and $GDH_{E170K/Q252L}$ (13.8-55 g/L) and $NAD^+$ (0.5 mM). The reaction temperature was kept at 30°C or 40°C, and the pH was adjusted to 7.5 by titrating $Na_2CO_3$.

Samples were withdrawn periodically, and extracted with ethyl acetate (EtAc). Centrifugation (12,000 × g, 10 min) was carried out to facilitate the separation of two phases. The organic layer was dehydrated using anhydrous $Na_2SO_4$ and then subjected to GC analysis (Agilent 7820A system) with the HP-5 column to determine the conversion and yield. Otherwise, the samples were heated to remove EtAc, re-dissolved in isopropanol and then filtered with filter membranes (0.22 μm) for chiral HPLC analysis with chiral column OD-H for determination of enantiomeric excess (*ee*) value under the following conditions: detection wavelength of 210 nm, flow rate of 1.0 mL/min, n-hexane : isopropanol volume ratio of 98:2. The absolute configuration of products was compared according to authentic standards or literature reports [11,26,39]. The retention time of (*S*)- and (*R*)-HPBE was 12.7 min and 18.4 min, respectively (Fig. S1). The HPLC detection limit (DL) of (*R*)- and (*S*)-HPBE were 0.03 and 0.02 mM, and their quantitation limit (QL) were 0.09 and 0.08 mM, respectively. The product from reduction of OPBE by mut-W913L/C93I/I187L was confirmed by $^1H$ NMR ($CDCl_3$, 500 Hz): δ=1.38 (3H, t; $OCH_2CH_3$), 1.99-2.10 (1H, m; $ArCH_2CHH$), 2.17-2.27 (1H, m; $ArCH_2CHH$), 2.80-2.93 (2H, m; $ArCH_2$), 3.16 (1H, s; O*H*), 4.25-4.36 (3H, m; $OCH_2CH_3$, C*H*OH) , 7.25-7.42 (5H, m; Ar-*H*) (Fig. S2).

## Results and discussion

**Computer-aided mutation of carbonyl reductase *Go*CR**

Our previous study revealed that residue Trp193 located in the substrate-binding pocket plays a critical role in determining the stereoselectivity of carbonyl reductase *Go*CR via a computational strategy [26]. Herein, residue Trp193 that might affect the stereoselectivity and activity were analysed in detail by

**Table 1.** Stereoselectivity and specific activity of wild-type *Go*CR and its variants at 193 site.

| Mutants | ee value (%, *R*) | Specific activity (U/mg) | Improved fold |
|---|---|---|---|
| **WT** | 43.0 | 3.7 ± 0.3 | 1 |
| **W193A** | 99.3 | 16.3 ± 0.6 | 4.4 |
| **W193L** | 99.1 | 18.4 ± 0.7 | 5.0 |
| **W193I** | 99.2 | 14.0 ± 1.1 | 3.8 |
| **W193V** | 99.1 | 14.7 ± 0.5 | 4.0 |
| **W193F** | 96.3 | 13.0 ± 0.8 | 3.5 |
| **W193M** | 98.6 | 3.8 ± 0.2 | 1.0 |
| **W193N** | 98.2 | 2.4 ± 0.5 | 0.6 |
| **W193P** | 97.9 | 9.3 ± 0.8 | 2.5 |
| **W193Q** | 98.4 | 4.7 ± 0.3 | 1.3 |
| **W193S** | 98.3 | 5.9 ± 1.1 | 1.6 |
| **W193T** | 97.7 | 1.3 ± 0.2 | 0.4 |
| **W193G** | 98.5 | 3.1 ± 0.5 | 0.8 |
| **W193Y** | 98.6 | 4.3 ± 0.7 | 1.2 |
| **W193C** | 98.5 | 4.8 ± 0.3 | 1.3 |

semisaturation mutagenesis. Considering that the substrate-binding pocket of *Go*CR is electrically neutral, a smart mutant library of non-charged amino acid substitutions at 193 site was constructed and screened for concurrent improvements in stereoselectivity and enzyme activity. SDS-PAGE analysis showed that all variants were expressed in soluble form in *E. coli* cells with molecular weights (MW) about 28 kDa, similar to the wild-type *Go*CR (Fig. S3). As shown in Table 1, all variants in the mutant library exhibited significantly improved stereoselectivity compared to wild-type *Go*CR. Among them, in addition to the previously reported mut-W193A [26], three variants, W193L (named as mut-W193L), W193I (mut-W193I) and W193V (mut-W193V), also showed the highest stereoselectivity of >99%. Moreover, it was noted that Trp193 residue was also identified as a potential 'hotspot' for improving enzyme activity. Most variants exhibited higher activity than the wild-type *Go*CR, especially the variant mut-W193L had the highest enzyme activity of 18.4 U/mg, exhibiting a 5.0-fold improvement compared to the wild-type *Go*CR. Taken stereoselectivity and enzyme activity into consideration, mut-W193L was chosen to further improve its catalytic efficiency towards OPBE.

The computational method including molecular docking and Molecular Mechanics Generalized Born Surface Area (MM-GBSA) method was used to identify potential residues for improving enzyme activity of mut-W193L. As shown in Fig. 1a, molecular docking analysis revealed that the substrate OPBE was accurately located at the substrate-binding pocket of mut-W193L, which further confirmed that OPBE could be reduced by mut-W193L. Subsequently, 22 residues (Cys93, Ser142, Ile143, Ala144, Gly145, Glu147, Gly148, Tyr149, Leu152, Tyr155, Pro185, Gly186, Ile187, Val188, Met192, Leu193, Ile196, Lys213, Lys214, Tyr215, Val216, Leu256) in the vicinity of 4 Å from the substrate OPBE were selected for the per-residue binding free energy calculated by the MM-GBSA method to discern the 'hotspots' in mut-W193L. According to the reported study, binding free energy values $\triangle G_{bind}$ >-1.0 kcal/mol was identified as major contributors to the substrate binding [40]. Accordingly, five residues (Cys93, Ser142, Tyr155, Ile187 and Leu193) were chosen as candidate sites for affecting substrate binding due to relatively high binding free energy values ($\triangle G_{bind}$ >-1.0 kcal/mol) (Fig. 1b). Among these residues, Ser142 and Tyr155 are significant catalytic residues in the conserved catalytic tetrad (Asn113-Ser142-Tyr155-Lys159) of mut-W193L, and the Leu193 site has been modified previously. These three amino acid residues were therefore excluded from mutagenesis. Therefore, another two residues (Cys93 and Ile187) in the substrate-binding pocket (Fig. 1c) were chosen as target sites for saturation mutagenesis and subsequent combination of beneficial mutations.

After being expressed in *E. coli* BL21 (DE3), all variants were similar to mut-W193L in protein expression, indicating that residue substitutions of 93 site and 187 site did not affect protein expression (Fig. S4 and S5). After screening of the saturation mutation library at 93 site, eight double-site variants (mut-W193L/C93I, mut-W193L/C93L, mut-W193L/C93F, mut-W193L/C93S, mut-W193L/C93Q, mut-W193L/C93T, mut-W193L/C93Y, mut-W193L/C93G) exhibiting 1.1- to 2.2-fold improvements in catalytic activity were identified compared with single-site variant mut-W193L, indicating 93 residue could affect enzyme activity (Fig. 2a). For the mutants at 187 site, four hits (mut-W193L/I187F, mut-W193L/I187L, mut-W193L/I187S, mut-W193L/I187V) exhibited obvious enhancement in catalytic activity relative to single-site variant mut-W193L, which revealed that 187 site was another hotspot for affecting enzyme activity (Fig. 2b). These results further verified our above prediction that 93 and 187 sites could obviously affect the interaction between enzyme and substrate. Among them,

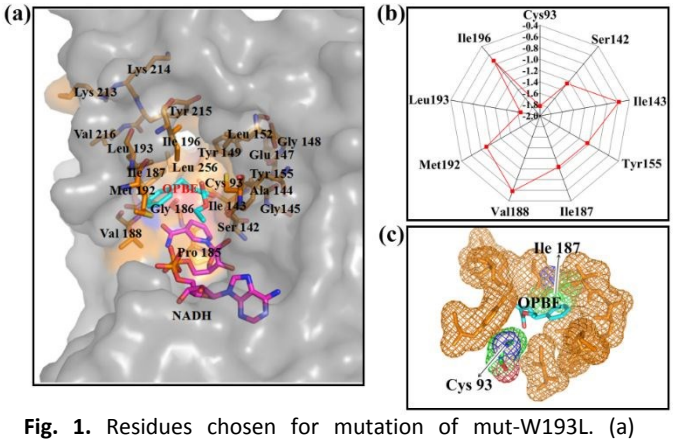


**Fig. 1.** Residues chosen for mutation of mut-W193L. (a) Residues (in orange) within the substrate-binding pocket of mut-W193L within a 4 Å vicinity of the substrate OPBE. (b) Per-residue binding free energy calculated by the MM-GBSA method for mut-W193L-OPBE complex. Only negative $\Delta G_{bind}$ value of residues contributing to the binding of OPBE are displayed. (c) The candidate sites (Cys93 and Ile187) in substrate-binding pocket of mut-W193L for mutation.

View Article Online
DOI: 10.1039/D0CY01411G

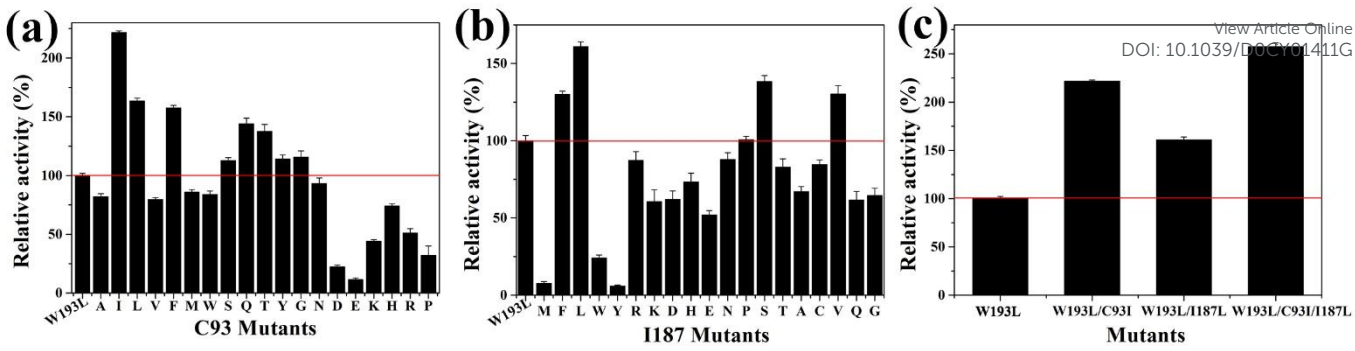


**Fig. 2.** Relative activities of mutants as compared to that of the mut-W193L. (a) C93 site mutants, (b) I187 site mutants and (c) optimal double-site variants and three-site variant.

the best double-site variants mut-W193L/C193I and mut-W193L/I187L exhibited 2.2 and 1.6 times as catalytic activity as the mut-W193L, respectively. Cooperative mutational and additivity effects are often adopted to further improve catalytic activity when simplifying protein engineering [41]. Hence, the mut-W193L/C93I and mut-W193L/I187L were attempted to combine for increasing activity. As expected, variant mut-W193L/C93I/I187L displayed a 1.2- and 1.6-fold further increase in catalytic activity in comparison to mut-W193L/C93I and mut-W193L/I187L, respectively (Fig. 2c). The stereoselectivity of the best variant mut-W193L/C93I/I187L toward OPBE remained >99% *ee*.

**Analysis of mutants with increased catalytic activity from kinetics and structural perspective**

To comparatively evaluate catalytic efficiency and elucidate the reason for the increase in activity from kinetics perspective, the specific activities and kinetic parameters of the purified wild-type *Go*CR and its variants with increased catalytic activity were determined (Table 2 and Fig. S6). In comparison with the wild-type *Go*CR, all variants exhibited a great improvement in specific activity toward OPBE (Table 2), which was consistent with the increased catalytic activities of these variants (Fig. 2). Correspondingly, single-site mutation (mut-W193L), double-site mutation (mut-W193L/C93I, mut-W193L/I187L) and triple-site mutation (mut-W193L/C93I/I187L) exhibited a progressive increase in catalytic efficiency ($k_{cat}/K_m$) compared to *Go*CR. Moreover, the enhancement in $k_{cat}/K_m$ was attributed to the decrease in $K_m$ and the increase in $k_{cat}$. It was noted that the introduction of Leu substitution of Trp193 made an important contribution to the increased activity and the increased catalytic efficiency, affording a 5.0-fold increase in specific activity and 9.8-fold increase in $k_{cat}/K_m$ toward OPBE in comparison with wild-type *Go*CR (Table 2, entry 1, 3). Subsequently, compared with the starting mut-W193L, mut-W193L/C93I and mut-W193L/I187L displayed 3.6- and 1.9-fold further increase in $k_{cat}/K_m$, respectively (Table 2, entry 3, 4, 5). The enhanced $k_{cat}/K_m$ of mut-W193L/C93I thus improved specific activity mainly benefit from the decreased $K_m$ and increased $k_{cat}$. The combinational mutations of W193L/C93I with W193L/I187L resulted in clearly additivity effects on activity. The resulting variant (mut-W193L/C93I/I187L) exhibited the highest specific activity and the most enhanced $k_{cat}/K_m$ value, which mainly benefited from a decrease in $K_m$ value together with an increase in $k_{cat}$ value (Table 2, entry 6). Furthermore, mut-W193L/C93I/I187L exhibited 5.3-fold higher catalytic efficiency compared to that of reported mut-W193A (Table 2, entry 2, 6), due to the decreased $K_m$ and increased $k_{cat}$. In general, mut-W193L/C93I/I187L exhibited a 14.0-fold enhancement in specific activity and a 37.0-fold increase in $k_{cat}/K_m$ compared to wild-type *Go*CR (Table 2, entry 1, 6).

**Table 2.** Specific activity and kinetic parameters of *Go*CR and its variants towards OPBE.

| Entry | Mutants | Specific activity (U/mg) | $K_m$ (mM) | $k_{cat}$ ($s^{-1}$) | $k_{cat}/K_m$ ($mM^{-1}s^{-1}$) |
|---|---|---|---|---|---|
| 1 | *Go*CR | 3.7 ± 0.3 | 0.87 ± 0.08 | 1.96 ± 0.43 | 2.25 |
| 2 | W193A | 16.3 ± 0.6 | 0.53 ± 0.05 | 8.29 ± 1.35 | 15.64 |
| 3 | W193L | 18.4 ± 0.7 | 0.46 ± 0.04 | 10.10 ± 1.5 | 21.96 |
| 4 | W193L/C93I | 43.5 ± 2.2 | 0.27 ± 0.07 | 21.21 ± 2.84 | 78.56 |
| 5 | W193L/I187L | 33.9 ± 1.6 | 0.44 ± 0.04 | 18.52 ± 1.72 | 42.09 |
| 6 | W193L/C93I/I187L | 51.7 ± 2.9 | 0.31 ± 0.03 | 25.78 ± 2.11 | 83.16 |

Moreover, the mechanism for the enhancement of catalytic activity regarding amino acid substitutions was also explored at atomic level. Thus, molecular docking between *Go*CR or its variants and substrate was performed. According to the carbonyl reductase *Go*CR reaction mechanism, catalytic residue Tyr155 and NADH donated their hydrogen atoms to the carbonyl oxygen and stereogenic carbon atom of substrate OPBE, respectively, resulting in the reduction of OPBE (Fig. 3a). Thus, the Distance 1 was defined as the distance between the stereogenic carbonyl carbon atom of OPBE and a hydrogen from the $C_4$ atom of the nicotinamide ring of NADH. The Distance 2 was defined as the distance between the carbonyl oxygen atom of OPBE and the hydroxyl group of Tyr155. Both Distance 1 and Distance 2 played key roles in determining the catalytic activity of enzyme towards the substrate OPBE. For *Go*CR, the Distance 1 and Distance 2 were 4.4 Å and 3.8 Å, respectively (Fig. 3b and Table S3, entry 1), indicating the stable catalytic conformation was not easily achieved. After mutation of Trp at 193 site to Leu, the Distance 1 and

View Article Online
DOI: 10.1039/D0CY01411G

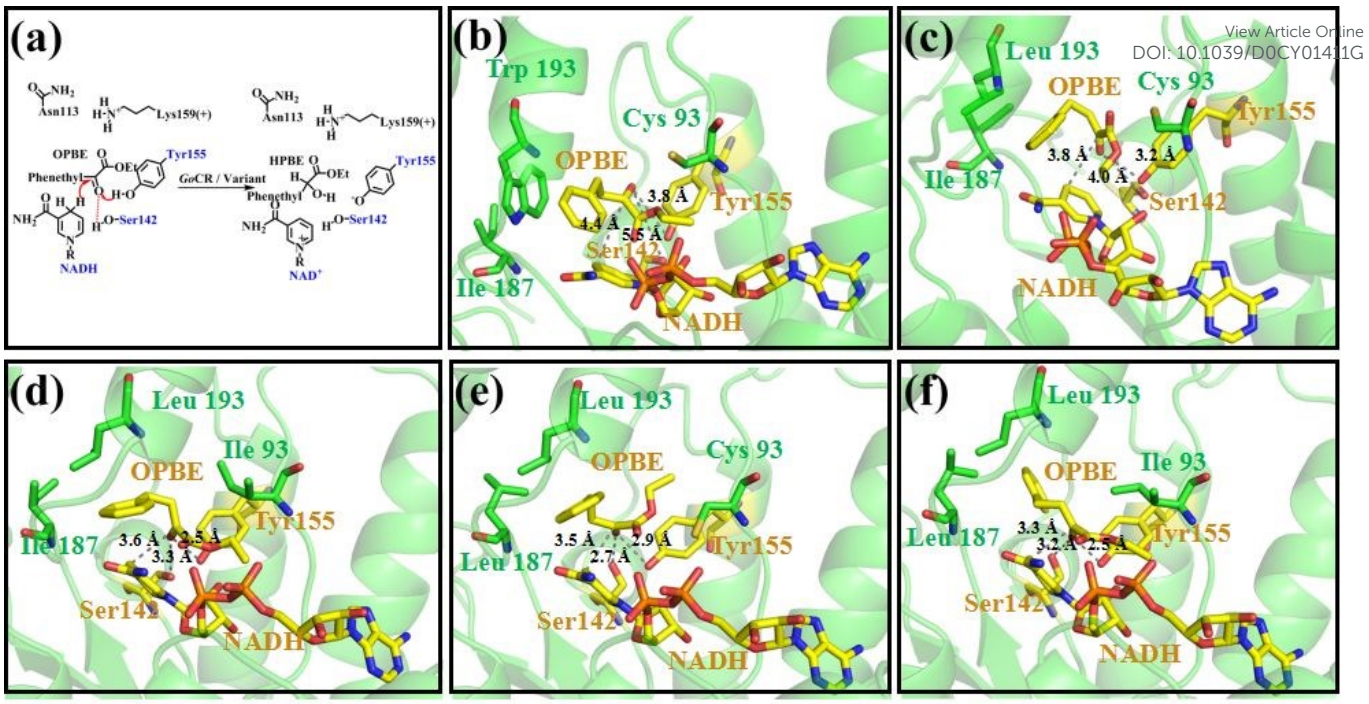


**Fig. 3.** (a) Proposed catalytic mechanism of *Go*CR and its variants for the reduction of OPBE; Molecular docking of OPBE into the active sites of *Go*CR and its variants towards OPBE. (b) *Go*CR, (c) mut-W193L, (d) mut-W193L/C93I, (e) mut-W193L/I187L and (f) mut-W193L/C93I/I187L.

Distance 2 was shorten to 3.8 Å and 3.2 Å, respectively (Fig. 3c and Table S3, entry 2). Subsequently, compared with mut-W193L, the Distance 1 in mut-W193L/C93I, mut-W193L/I187L and mut-W193L/C93I/I187L was obviously shortened (Fig. 3d, 3e, 3f and Table S3, entry 3-5), which benefited nucleophilic attack on stereogenic carbonyl carbon atom of OPBE. Meanwhile, the Distance 2 in mut-W193L/C93I, mut-W193L/I187L as well as mut-W193L/C93I/I187L were also shortened to within 2.9 Å, which was beneficial for the reduction of carbonyl oxygen atom of OPBE. Additionally, Ser142 can stabilize substrate or transition state of intermediate through hydrogen bond (H-bond) between carbonyl oxygen atom of OPBE and hydroxyl groups of Ser142 (Fig. 3a). The *Go*CR could not form a stable H-bond with substrate OPBE because the Distance 3 between carbonyl oxygen atom of OPBE and hydroxyl groups of Ser142 was 5.5 Å, which was longer than 3.5 Å that is the threshold for forming a stable H-bond (Fig. 3b and Table S3, entry 1). Furthermore, for mut-W193L, the stable H-bond between Ser142 and OPBE still could not be formed (Fig. 3c and Table S3, entry 2), thus the stable transition states of intermediate could not occur. After further mutation at 93 site and 187 site, such distance in all three mutants was shortened to within 3.3 Å (Fig. 3d, 3e, 3f and Table S3, entry 3-5), therefore stable H-bond could be formed which could stabilize the transition states of intermediate. It was also part of main reason for the increase in catalytic activity. Therefore, mutants at the 93 site and 189 site (mut-W193L/C93I, mut-W193L/I187L, mut-W193L/C93I/I17L) chosen by structural-guide analysis significantly improved enzyme catalytic activity by shortening the distances of OPBE with NADH and with key catalytic residues in substrate-binding pocket.

**Thermostability analysis of *Go*CR variants**

Given that there is sometimes a trade-off between enzymatic activity and enzyme stability [30,42], the thermostabilities in terms of melting point ($T_m$) of *Go*CR and four variants (mut-W193L, mut-W193L/C93I, mut-W193L/I187L and mut-W193L/C93I/I187L) were determined by CD measurements. Fig. S7 and Fig. S8 showed that *Go*CR and its variants exhibited double minimal negative peaks at approximately 208 nm and 222 nm, implying abundant $\alpha$-helixs in *Go*CR and its variants, which are consistent with the crystal structure of *Go*CR (PDB ID: 3WTC) [26]. As the temperature increased, the CD values at 208 and 222 nm for the tested variants gradually decreased, indicating the unfolding of protein increased, which was due to the destroyed secondary structure. The $T_m$ values of mut-W193L/C93I, mut-W193L/I187L and mut-W193L/C93I/I187L were 62.4, 60.3 and 70.7°C, respectively, higher than the mut-W193L ($T_m$ =58.8°C) (Fig. 4a and 4b). Thus, both thermostability and catalytic activity of the engineered mut-W193L/C93I, mut-W193L/I187L and mut-W193L/C93I/I187L were improved compared to mut-W193L. Besides, although the thermostability of mut-W193L and mut-

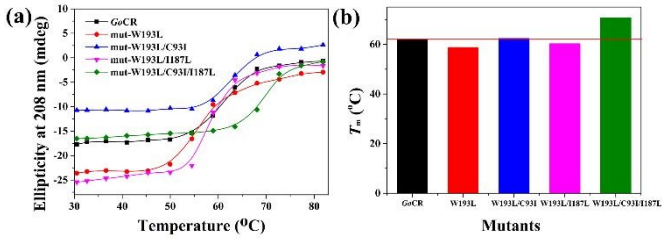


**Fig. 4.** CD analysis of *Go*CR and its variants (a) Thermal denaturation of *Go*CR and its variants by CD spectra; (b) Melting temperature ($T_m$) of *Go*CR and its variants.

W193L/I187L had slightly decreased and mut-W193L/C93I did not change a lot compared to wild-type *Go*CR ($T_m$ = 62.1°C), mut-W193L/C93I/I187L exhibited obviously increased thermostability (Fig. 4b). It is worth noting that mut-W193L/C93I/I187L with the highest enzyme activity showed the highest thermostability. The $T_m$ value of mut-W193L/C93I/I187L was enhanced by 8.6°C compared to the wild-type *Go*CR. As we known, in addition to the increased catalytic activity, excellent thermostability of enzyme is also preferable in large-scale industrial processes, because higher reaction temperature often effectively lowered the risk of contamination, improved mass transfer rate and promoted the solubility of poorly dissolved substrates [43]. In the past few decades, numerous successful examples have been reported for improving the thermostability of enzymes by directed evolution or (semi-) rational design [43-45]. In these studies, the mutation sites selected are usually far away from the active pocket or have no direct interaction with the substrate. In our study, the best variant mut-W193L/C93I/I187L with significant improvement in both catalytic efficiency and thermostability was obtained by engineering the amino acid residues in the substrate-binding pocket, which had direct interaction with substrate.

In order to elucidate the mechanism of increased thermostability, the major intramolecular interactions, such as the Van der Waals's interactions, salt bridges, hydrogen bonds and disulphide bond that are considered as the dominant structural factors responsible for protein thermostability, were analyzed using the RING 2.0 web server [46]. As shown in Fig. 5, 93 and 187 sites are located on flexible loop8 and loop12 surrounding the active site residues, respectively. Compared with the model structure of mut-W193L, mut-W193L/C93I revealed that two new van der Waals interaction were formed by Ile93 and Ile196 located on helix $\alpha$7, and by Ile187 with Leu193 located on helix $\alpha$7 (Fig. 5a and 5b). Additional I187L mutation in mut-W193L formed a new van der Waals interaction by Ile187 with Leu193 located on helix $\alpha$7 (Fig. 5a and 5c). All the above van der Waals interactions were observed in mut-W193L/C93I/I187L, besides, another new van der Waals interaction formed by Ile187 with Tyr212 located on helix $\alpha$8 (Fig. 5a and 5d). Together, these additional van der Waals interaction increased the stability of flexible loop8 and loop12 surrounding the active site residues, which might account for the significantly increased melting temperature of mut-W193L/C93I, mut-W193L/I187L and mut-W193L/C93I/I187L in comparison with the mut-W193L. Similar phenomenon also could be observed in Gong's study [41]. Besides, the increased thermostability of mut-W193L/C93I/I187L in comparison with wild-type *Go*CR might be due to the further enhanced stability of flexible loop8 (Fig. 5d and Fig. S9), which resulted from the new van der Waals interaction formed by Ile93 and Ile196 located on helix $\alpha$7.

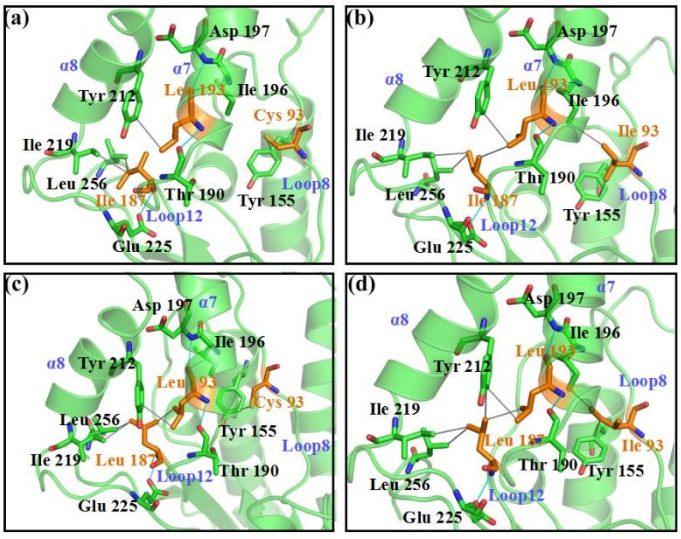


**Fig. 5.** Local residue interactions of *Go*CR variants predicted by the RING 2.0 web server. (a) mut-W193L, (b) mut-W193L/C93I, (c) mut-W193L/I187L and (d) mut-W193L/C93I/I187L. The hydrogen bonds and Van der Waals interactions are indicated by light blue and gray lines, respectively.

### Synthesis of (*R*)-HPBE using engineered variants

To further evaluate the feasibility of biocatalytic process at high substrate loading, asymmetric reduction of OPBE to (*R*)-HPBE was performed using lyophilized recombinant *E. coli* cells overexpressing *Go*CR variants (mut-W193L, mut-W193L/C93I, mut-W193L/I187L or mut-W193L/C93I/I187L) and $GDH_{E170K/Q252L}$ for the regeneration of NADH in situ (Fig. 6a and Fig. S10). The variants mut-W193L/C93I, mut-W193L/I187L and mut-W193L/C93I/I187L continued to display pronounced catalytic activity towards OPBE compared to mut-W193L which exhibited low conversion of about 68.5% within 22 h (Fig. 6b and Table 3, entry 3). Among these variants, mut-W193L/C93I/I187L displayed the highest reaction rate towards 1.5 M OPBE, completing conversion within 12 h, followed by mut-W193L/C93I within 16 h. The mut-W193L/I187L also converted over 99% of 1.5 M OPBE within 22 h (Fig. 6b and Table 3, entry 4-6). The specific activity of mut-W193L/C93I/I187 was the highest among the *Go*CR variants; it is therefore reasonable that its catalytic efficiency were higher than those of the other three variants in the trial. Moreover, mut-W193L/C93I/I187 also exhibited higher catalytic efficiency than the reported mut-W193A, which was consistent with the above results of specific activity (Table 3, entry 2, 6). Although all variants exhibited different catalytic efficiency, they displayed

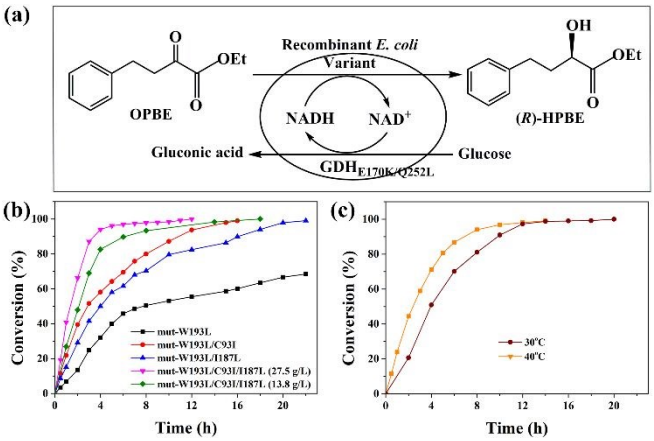


**Fig. 6.** Time courses of reduction of OPBE by variants. (a) Representative asymmetric reduction of OPBE by variants; (b) Time course of reduction of 1.5 M OPBE by mut-W193L, mut-W193L/C93I, mut-W193L/I187L or mut-W193L/C93I/I187L; (c) Time courses of reduction of 1.8 M OPBE by mut-W193L/C93I/I187L at different temperatures (30°C and 40°C).

View Article Online
DOI: 10.1039/D0CY01411G





**Table 3.** Asymmetric reduction of OPBE catalyzed by *Go*CR or its variants.

| Entry | Biocatalyst | OPBE (M) | S/C ratio (g/g)[d] | Temperature (°C) | Time(h) | Conversion (%) | *ee* (%) |
|---|---|---|---|---|---|---|---|
| **1** | **WT**[a] | 1.5 | 5.6 | 30 | 20 | 9.7 | 43.0 |
| **2** | **W193A** | 1.5 | 11.2 | 30 | 24 | 39.2 | 99.2 |
| **3** | **W193L**[a] | 1.5 | 11.2 | 30 | 22 | 68.5 | 99.3 |
| **4** | **W193L/I187L**[a] | 1.5 | 11.2 | 30 | 22 | >99 | 99.4 |
| **5** | **W193L/C93I**[a] | 1.5 | 11.2 | 30 | 16 | >99 | 99.3 |
| **6** | **W193L/C93I/I187L**[a] | 1.5 | 11.2 | 30 | 12 | >99 | 99.4 |
| **7** | **W193L/C93I/I187L**[b] | 1.5 | 22.4 | 30 | 18 | >99 | 99.2 |

[a] Reaction condition: OPBE (309 g/L), D-glucose (1.2 equiv.), lyophilized *E. coli* cells co-expressing $GDH_{E170K/Q252L}$ and *Go*CR (55 g/L) or its variants (27.5 g/L), octanol (15%) and $NAD^+$ (0.5 mM). The reaction temperature was kept at 30°C.
[b] Reaction condition: OPBE (309 g/L), D-glucose (1.2 equiv.), lyophilized *E. coli* cells co-expressing $GDH_{E170K/Q252L}$ and mut-W193L/C93I/I187L (13.8 g/L), octanol (15%) and $NAD^+$ (0.5 mM). The reaction temperature was kept at 30°C.
[c] Reaction condition: OPBE (371 g/L), D-glucose (1.2 equiv.), lyophilized *E. coli* cells co-expressing $GDH_{E170K/Q252L}$ and mut-W193L/C93I/I187L (13.8 g/L), octanol (15%) and $NAD^+$ (0.5 mM). The reaction temperature was kept at 30 or 40°C.
[d] S/C: substrate/catalyst ratio

| | | | | | | | |
|---|---|---|---|---|---|---|---|
| **8** | **W193L/C93I/I187L**[c] | 1.8 | 26.9 | 30 | 20 | >99 | 99.1 |
| **9** | **W193L/C93I/I187L**[c] | 1.8 | 26.9 | 40 | 14 | >99 | 99.2 |

excellent stereoselectivity toward OPBE and afforded (*R*)-HPBE with >99% *ee* (Table 3, entry 2-6).

Although the variant mut-W193L/C93I/I187L displayed excellent activity, the observed substrate/catalyst (S/C) ratio of 11.2 g/g was still low (Table 3, entry 6). When the cell concentration was reduced to 13.8 g/L of lyophilized *E. coli* cells, affording the increased S/C ratio of 22.4 g/g, the reaction at a substrate loading of 1.5 M was accomplished completely within 18 h by mut-W193L/C93I/I187L (Fig. 6b and Table 3, entry 7). Excitingly, even at a higher substrate loading of 1.8 M, a complete conversion was also achieved in 20 h with the catalyst loading of 26.9 g/g (Fig. 6b and Table 3, entry 8).

Given that thermostability of mut-W193L/C93I/I187L was increased significantly, and the half-life of mut-W193L/C93I/I187L at 40°C was 19.3 h (Fig. S11), we attempted to carry out the reduction of OPBE by mut-W193L/C93I/I187L at higher temperature of 40°C, instead of 30°C, in order to shorten the reaction time. As shown in Fig. 6c and Table 3, entry 8, 9, 1.8 M OPBE could be completely converted at 40°C within the shorter time of 14 h compared to 20 h at 30°C. This result highlighted the considerable operational stability of mut-W193L/C93I/I187L under the reaction conditions, which is in agreement with its high $T_m$ value. To sum up, several mutants with excellent catalytic efficiency were successfully constructed through the semi-rational strategy. As a result, the catalyst loading S/C ratio ($g_{substrate}/g_{catalyst}$) was dramatically increased from 5.6 to 26.9 g/g, and the substrate concentration which could be completely reduced by the best mut-W193L/C93I/I187L was significantly enhanced to 1.8 M (371 g/L), resulting in >99% *ee* and 540.4 g/(L·day) space-time yield. It is noteworthy that a substrate loading with >99% conversion in this study reached 371 g/L, which was higher than the highest record reported so far for the reduction of OPBE to produce (*R*)-HPBE (Table S4). These results showed the excellent catalytic activity and potential application of variant mut-W193L/C93L/I187L for production of (*R*)-HPBE.

**Substrate spectrum of mut-W193L/C93I/I187L**

**Table 4.** Carbonyl compounds with different molecular volumes catalyzed by mut-W193L/C93I/I187L.

| Entry | Substrate | Volume (Å) | Conv.(%) | *ee* (%) |
|---|---|---|---|---|

View Article Online
DOI: 10.1039/D0CY01411G

| | | | | | |
|---|---|---|---|---|---|
| **1** | 2'-Fluoroacetophenone |  | 127.18 | >99[a] | >99 (S) |
| **2** | 2'-Bromoacetophenone |  | 143.31 | >99[a] | >99 (S) |
| **3** | 4'-Chloroacetophenone |  | 137.62 | >99[a] | >99 (S) |
| **4** | Ethyl benzoylformate | 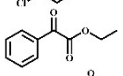 | 178.53 | >99[b] | >99 (R) |
| **5** | 3',5'-Bis(trifluoromethyl)acetophenone | 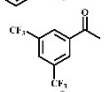 | 196.37 | >99[a] | >99 (S) |
| **6** | ethyl 2-Oxo-4-phenyl-butyrate | 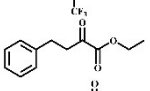 | 210.04 | >99[a] | >99 (R) |
| **7** | 2-Oxo-4-phenylbutyric acid | 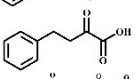 | 170.58 | N.A.[b,c] | -- |
| **8** | (4*S*)-3-[5-(4-fluorophenyl)-1,5-dioxophentyl]-4-phenyl-1, 3-oxazolidin-2-one | 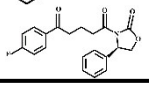 | 342.82 | N.A.[b,c] | -- |

[a] 100 mM substrate concentrate.
[b] 10 mM substrate concentrate.
[c] No measurable activity.

In order to further evaluate the application potential of mut-W193L/C93I/I187L, we explored a panel of substrates and found that mut-W193L/C93I/I187L displayed a broad substrate spectrum, notably exhibiting higher reduction activity towards *α*-diketones (Table S5). Compared with wild-type *Go*CR, mut-W193L/C93I/I187L showed a general improvement in catalytic efficiency toward the tested substrates, with the exceptions of 2, 3-Butanedione and 2-Pentanone. In addition, we observed that mut-W193L/C93I/I187L tended to reduce the ketones with bulky aromatic side chains. Thus, mut-W193L/C93I/I187L can serve as an attractive and versatile biocatalyst in the reduction of ketone substrates. Considering that mut-W193L/C93I/I187L exhibited high activity towards aromatic ketones, we also tested a panel of aromatic ketones with various molecular volumes as substrates to further examine the enzymatic performance of mut-W193L/C93I/I187L. The results showed that aromatic ketone and ketone ester substrates with volume ranging from 127.18-210.04 Å could be efficiently and stereo-selectively reduced by mut-W193L/C93I/I187L (Table 4), thereby indicating its strong catalytic performance with bulky aromatic ketone and ketone ester substrates. In contrast, no detectable activity was observed towards aromatic keto acid (Table 4, entry 7) or the bulky diaryl ketone (Table 4, entry 8). In conclusion, mut-W193L/C93I/I187L exhibited a broad substrate spectrum and high catalytic activity towards bulky substrates, indicating its versatility and potential applications as a catalyst in the preparation of chiral alcohols.

## Conclusions

In this study, the key residue Cys93 responsible for stereoselectivity and enzyme activity, as well as Ile187 and Trp193 site that played the role in determining the enzyme activity of *Go*CR were identified, based on computational approach in combination with semisaturation/saturation mutagenesis. Subsequently, four *Go*CR variants that exhibited simultaneous enhancement in catalytic activity and stereoselectivity toward OPBE compared with the wild-type enzyme were successfully obtained using single-site mutation and cooperative mutation. The variants mut-W193L, mut-W193L/C93I, mut-W193L/I187L and mut-W193L/C93I/I187L showed the excellent stereoselectivities with >99% *ee* compared to 43.0% of the wild-type *Go*CR. Among these variants, mut-W193L/C93I/I187L showed the highest specific activity and catalytic efficiency, which were enhanced by 14.0- and 37.0-fold, respectively, compared to the wild-type *Go*CR. It was noted that the simultaneous enhancement in thermostability was occurred on the variant mut-W193L/C93I/I187L. The $T_m$ of mut-W193L/C93I/I187L was improved to 70.7°C from 62.1°C of the wild-type *Go*CR. Structural analysis of variant revealed that the obvious shortened distances of substrate with nicotinamide cofactor NADH and with catalytic residues Ser142 and Tyr155 in these four variants accounted for the increased catalytic activity. Additionally, three additional van der Waals interactions stabilize flexible loop 8 and loop 12 around the active sites, leading to an 8.6°C improvement in thermostability when compared with wild-type *Go*CR. Most importantly, at an elevated temperature of 40°C, as high as 1.8 M OPBE could be completely reduced with >99% *ee* and 540.4 g/(L·day) space-time yield, indicating the great potential of mut-W193L/C93I/I187L for preparative synthesis of (*R*)-HPBE.

## Conflicts of interest

There are no conflicts to declare.

## Acknowledgements

This work was supported by Natural Science Foundation of Shanghai (No. 19ZR1412700), the Fundamental Research Funds for the Central Universities (No. 22221818014), Natural Science Foundation in Jiangsu Province (BK20160373) and partially supported by Open

Funding Project of the State Key Laboratory of Bioreactor Engineering.

## References

1 B. S. Chen and F. Z. R. de Souza, *RSC Adv.* 2019, **9**, 2102-2115.
2 Y. Nie, S. S. Wang, Y. Xu, S. G. Luo, Y. L. Zhao, R. Xiao, G. T. Montelione, J. F. Hunt and T. Szyperski, *ACS Catal.* 2018, **8**, 5145-5152.
3 Y. Zhou, Q. Y. Peng, L. Zhang, S. H. Cheng, L. T. Zeng, F. Dong and Z. Y. Yang, *Food Chem.* 2019, **280**, 27-33.
4 G.-C. Xu and Y. Ni, *Bioresour. Bioprocess.* 2015, **2**, 15.
5 P. Herold, A. F. Indolese, M. Studer, H. P. Jalett, U. Siegrist and H. U. Blaser, *Tetrahedron* 2000, **56**, 6497-6499.
6 Z. G. Wang, S. Zhou, S. L. Zhang, S. Zhang, F. M. Zhu, X. L. Jin, Z. M. Chen and X. L. Xu, *Sci. Rep-UK* 2017, **7**, 4007-4017.
7 S. H. Huang and S. W. Tsai, *J. Mol. Cata.l B-Enzym.* 2004, **28**, 65-69.
8 A. Liese, U. Kragl, H. Kierkels and B. Schulze, *Enzyme Microb. Tech.* 2002, **30**, 673-681.
9 T. Sugai and H. Ohta, *Agric. Biol. Chem.* 1991, **55**, 293-294.
10 W. Q. Lin, Z. He, Y. Jing, X. Cui, H. Liu and A. Q. Mi, *Tetrahedron-Asymmetr.* 2001, **12**, 1583-1587.
11 Y. Ni, Y. Su, H. Li, J. Zhou and Z. Sun, *J. Biotechnol.* 2013, **168**, 493-498.
12 Y. Chen, H. Lin, X. Xu, S. Xia and L. Wang, *Adv. Synth. Catal.* 2008, **350**, 426-430.
13 I. Kaluzna, A. A. Andrew, M. Bonilla, M. R. Martzen and J. D. Stewart, *J. Mol. Catal. B-Enzym.* 2002, **17**, 101-105.
14 Y. G. Shi, Y. Fang, H. P. Wu, F. Li and X. Q. Zuo, *Biocatal. Biotransfor.* 2009, **27**, 211-218.
15 I. Lavandera, A. Kern, M. Schaffenberger, J. Gross, A. Glieder, S. de Wildeman and W. Kroutil, *ChemSusChem* 2008, **1**, 431-436.
16 W. Zhang, Y. Ni, Z. H. Sun, P. Zheng, W. Q. Lin, P. Zhu and N. F. Ju, *Process Biochem.* 2009, **44**, 1270-1275.
17 N. D. Shen, Y. Ni, H. M. Ma, L. J. Wang, C. X. Li, G. W. Zheng, J. Zhang and J. H. Xu, *Org. Lett.* 2012, **14**, 1982-1985.
18 C. Li, R. Zhang, J. Wang, L. M. Wilson and Y. Yan, *Trends Biotechnol.* 2020, **38**, 729-744.
19 Z. Q. Liu, L. Wu, X. J. Zhang, Y. P. Xue and Y. G. Zheng, *J. Agr. Food Chem.* 2017, **65**, 3721-3729.
20 M. T. Reetz, *J. Am. Chem. Soc.* 2013, **135**, 12480-12496.
21 I. Stanzione, C. Pezzella, P. Giardina, G. Sannia and A. Piscitelli, *Appl. Microbiol. Biot.* 2020, **104**, 915-924.
22 L. Ba, P. Li, H. Zhang, Y. Duan and Z. L. Lin, *Biotechnol. Bioeng.* 2013, **110**, 2815-2825.
23 C. Zhang, Y. Liu, C. Li, Y. Xu, Y. Su, J. Li, J. Zhao and M. Wu, *Sci. Rep-UK* 2020, **10**, 1680-1691.
24 O. Spadiut, C. Leitner, C. Salaheddin, B. Varga, B. G. Vertessy, T. C. Tan, C. Divne and D. Haltrich, *FEBS J.* 2009, **276**, 776-792.
25 Y. Y. Xia, W. J. Cui, Z. Y. Cheng, L. Peplowski, Z. M. Liu, M. Kobayashi and Z. M. Zhou, *ChemCatChem* 2018, **10**, 1370-1375.
26 J. Deng, Z. Yao, K. Chen, Y. A. Yuan, J. Lin and D. Wei, *J. Biotechnol.* 2016, **217**, 31-40.
27 J. Vina-Gonzalez, D. Jimenez-Lalana, F. Sancho, A. Serrano, A. T. Martinez, V. Guallar and M. Alcalde, *Adv. Synth. Catal.* 2019, **361**, 2514-2525.
28 X. Liu, R. Chen, Z. W. Yang, J. L. Wang, J. P. Lin and D. Z. Wei, *Mol. Biotechnol.* 2014, **56**, 285-295.
29 M. M. Bradford, *Anal. Biochem.* 1976, **72**, 248-254.
30 F.-F. Chen, G.-W. Zheng, L. Liu, H. Li, Q. Chen, F.-L. Li, C.-X. Li and J.-H. Xu, *ACS Catal.* 2018, **8**, 2622-2628.
31 T. J. Hou, J. M. Wang, Y. Y. Li and W. Wang, *J. Comput. Chem.* 2011, **32**, 866-877.
32 A. Lindstrom, L. Edvinsson, A. Johansson, C. D. Andersson, I. E. Andersson, F. Raubacher and A. Linusson, *J. Chem. Inf. Model.* 2011, **51**, 267-282.
33 A. Weis, K. Katebzadeh, P. Soderhjelm, I. Nilsson and U. Ryde, *J. Med. Chem.* 2006, **49**, 6596-6606.
34 K. Wichapong, A. Rohe, C. Platzer, I. Slynko, F. Erdmann, M. Schmidt and W. Sippl, *J. Chem. Inf. Model.* 2014, **54**, 881-893.
35 T. Li, M. Froeyen and P. Herdewijn, *J. Mol. Graph. Model.* 2008, **26**, 813-823.
36 D. Piovesan, G. Minervini and S. C. E. Tosatto, *Nucleic Acids Res.* 2016, **44**, W367-W374.
37 B. Liang, Q. L. Lang, X. J. Tang and A. H. Liu, *Bioresource Technol.* 2013, **147**, 492-498.
38 E. Vazquez-Figueroa, J. Chaparro-Riggers and A. S. Bommarius, *ChemBioChem* 2007, **8**, 2295-2301.
39 R. Chen, J. Deng, J. P. Lin, X. P. Yin, T. Xie, S. L. Yang and D. Z. Wei, *Biotechnol. Appl. Bioc.* 2016, **63**, 465-470.
40 G. De Simone, E. Langella, D. Esposito, C. T. Supuran, S. M. Monti, J. Y. Winum and V. Alterio, *J. Enzym. Inhib. Med. Ch.* 2017, **32**, 1002-1011.
41 X. M. Gong, Z. Qin, F. L. Li, B. B. Zeng, G. W. Zheng and J. H. Xu, *ACS Catal.* 2019, **9**, 147-153.
42 N. Tokuriki, F. Stricher, L. Serrano and D. S. Tawfik, *PLoS Comput. Biol.* 2008, **4**, e1000002-e1000008.
43 L. J. Li, H. Liao, Y. Yang, J. Y. Gong, J. A. Liu, Z. D. Jiang, Y. B. Zhu, A. F. Xiao and H. Ni, *Int. J. Biol. Macromol.* 2018, **112**, 14-21.
44 W. Ren, L. Liu, L. Gu, W. L. Yan, Y. L. Feng, D. X. Dong, S. J. Wang, M. S. Lyu and C. H. Wang, *J. Agr. Food Chem.* 2019, **67**, 4355-4366.
45 H. J. Wijma, R. J. Floor and D. B. Janssen, *Curr. Opin. Struc. Biol.* 2013, **23**, 588-594.
46 X. Y. Wang, R. Ma, X. M. Xie, W. N. Liu, T. Tu, F. Zheng, S. You, J. Z. Ge, H. F. Xie, B. Yao and H. Y. Luo, *Sci. Rep-UK* 2017, **7**,15287-15295.

View Article Online
DOI: 10.1039/D0CY01411G

## Graphical Abstract

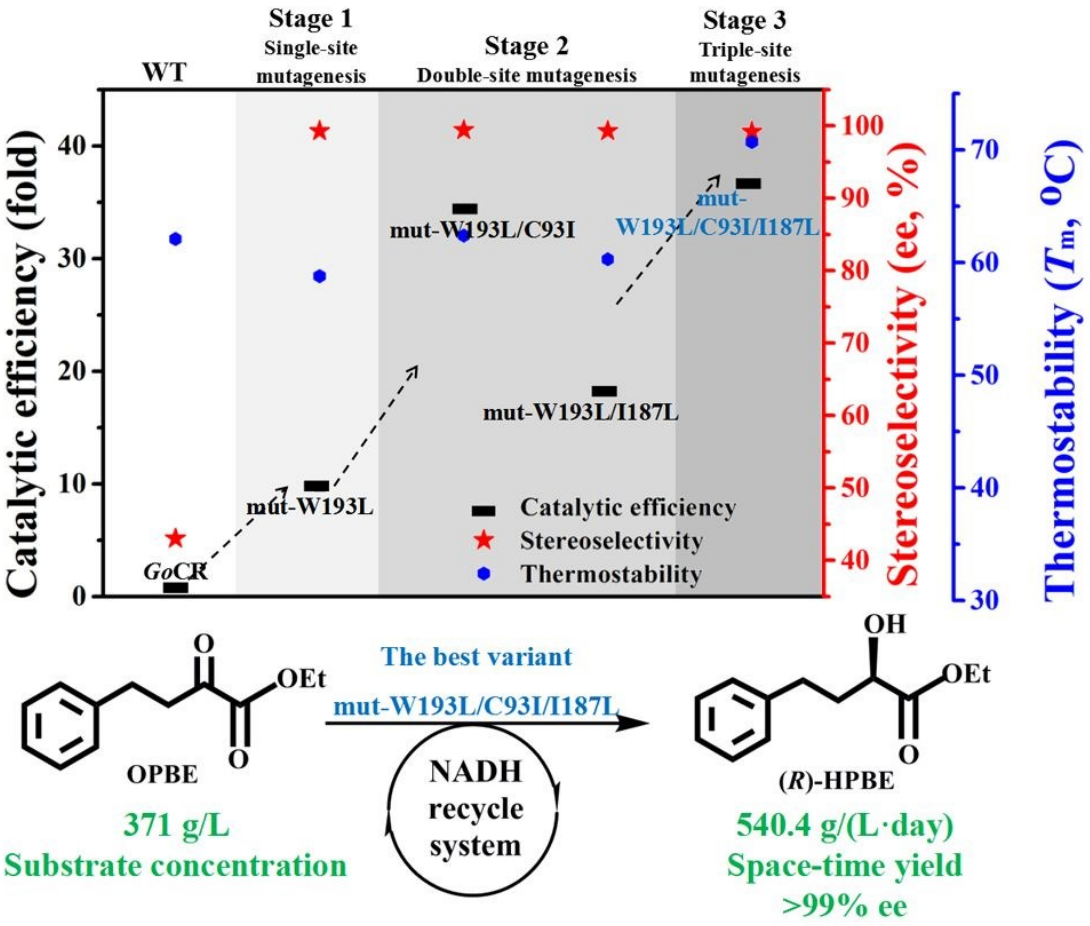


This study reported a highly efficient engineered carbonyl reductase from *Gluconobacter oxydans* (*Go*CR) through a structure-guided rational design to catalyze the synthesis of high concentration (*R*)-HPBE, which provided an attractive biocatalyst for the efficient synthesis of (*R*)-HPBE.